Site-Directed Spin-Labeling Study of the Structure and Subunit Interactions along a Conserved Sequence in the α-Crystallin Domain of Heat-Shock Protein 27. Evidence of a Conserved Subunit Interface†

Hassane S. Mchaourab,* Anderee R. Berengian, and Hanane A. Koteiche

National Biomedical ESR Center, Biophysics Research Institute, Medical College of Wisconsin, 8701 Watertown Plank Road, Milwaukee, Wisconsin 53226

Received July 14, 1997; Revised Manuscript Received September 2, 1997⊗

ABSTRACT: Site-directed spin-labeling (SDSL) was used to investigate the secondary structure, solvent accessibility, and tertiary and quaternary interactions along the sequence located between residues 133 and 144 in the α-crystallin domain of human heat-shock protein 27 (HSP 27). The sequence is conserved among mammalian sHSP and shows similarity to the region of highest homology between αA- and αB-crystallins. Eleven sequential single cysteine mutants were prepared and reacted with a sulfhydryl-specific spin-label. The accessibilities of attached nitroxide side chains to a paramagnetic probe in the aqueous solution were determined. Spectral line shapes were analyzed in terms of side-chain mobility and spatial proximity to nearby nitroxides. The sequence-specific mobilities and accessibilities varied with a period of 2, consistent with the presence of a *β*-strand along the sequence. At even sites, the nitroxide environment is highly ordered with virtually no accessibility to the hydrophilic probe, indicating that one face of the strand is buried. Furthermore, spin−spin interactions between nitroxides in the oligomeric structure strongly suggest that equivalent strands from different subunits are in close spatial proximity. These structural characteristics are remarkably similar to those of the equivalent sequence in αA-crystallin [Berengian, A. R., Bova, M. P., and Mchaourab, H. S. (1997) *Biochemistry 36*, 9951−9957]. In both proteins, a *β*-strand spans the sequence and is located at a subunit interface, indicating that one set of interactions between subunits, and its associated symmetry, is conserved. This is the first report of sequence-specific structural similarity between αA-crystallin and HSP 27 and the first identification of a conserved secondary structural element in the α-crystallin domain.

Small heat-shock proteins (sHSPs)[1] are one of four families of heat-shock proteins (HSPs) expressed in response to heat shock and other forms of stress (*1*). They are a diverse family of proteins that appear to be ubiquitous in nature, being found as surface antigens in eukaryotic parasites, as inclusion body-binding protein in *E. coli*, and as structural proteins in the vertebrate lens (*2*). Despite their low molecular mass (12−40 kDa), sHSPs are isolated as large oligomeric complexes of 12−40 subunits depending on the physiological state of the cell. Distant members of the family have relatively low sequence similarity except for a highly conserved stretch of 100 amino acids, often called the α-crystallin domain (*2*). Although their cellular function under physiological conditions is still largely unknown, the increased expression of sHSP is associated with cell survival under heat stress (*3*). The role of these proteins in thermotolerance appears to be a consequence of their ability to function as molecular chaperones and to modulate actin filament dynamics (*4*−*7*). sHSPs from many species inhibit the unfolding-induced aggregation of proteins in an ATP-independent manner and form a stable complex with their protein substrate. Thus, during periods of stress, sHSPs act as energy-independent traps preventing the irreversible aggregation of proteins. Recently, it has been shown that upon establishment of refolding conditions, proteins bound to sHSP are efficiently refolded in cooperation with other chaperones (*8, 9*).

Mammalian cells express two sHSPs: HSP 27 and αB-crystallin. In addition to their established role in thermotolerance, recent reports indicate that HSP 27 is involved in transduction pathways activated during oncoprotein-mediated neoplasticity (*10, 11*) in response to the cytotoxic effects of tumor necrosis factor α (TNF-α) (*12*), and in the regulation of apoptosis (*13*). This protective role is associated with phosphorylation-induced changes in the oligomeric state and intracellular localization of the protein (*14*). Both stress and growth stimulation lead to the phosphorylation of specific serine residues in HSP 27, suggesting that phosphorylation provides the coupling mechanism that regulates function via reorganization of the quaternary structure (*14*). Similar to human HSP 27, *Drosophila* HSP 27 and human αB-crystallin are able to protect against cell death induced by necrosis or apoptosis (*12*). Because the sequence similarity of sHSP is focused in the α-crystallin domain, it is logical to assume that this domain forms a common structural core (*15*), i.e., a region with similar secondary and tertiary structure, that

† Supported by Grants GM22923, EY01931, and RR01008 from the National Institutes of Health and a by grant from the Cancer Center of the Medical College of Wisconsin (ACS-IRG 170).

* Address correspondence to this author at the National Biomedical ESR Center, Biophysics Research Institute, Medical College of Wisconsin, 8701 Watertown Plank Rd., Milwaukee, WI 53226. Fax: (414) 456 6512. Email: hassane@mcw.edu.

⊗ Abstract published in *Advance ACS Abstracts,* November 15, 1997.

[1] Abbreviations: CD, circular dichroism; DTT, dithiothreitol; EPR, electron paramagnetic resonance; NiEDDA, nickel(II) ethylenediaminediacetate; PCR, polymerase chain reaction; SDSL, site-directed spin-labeling; sHSPs, small heat-shock proteins; T4L, T4 lysozyme; WT, wild type; HSP 27, heat-shock protein 27; TCEP tris(2-carboxyethyl)phosphine.

S0006-2960(97)01700-5 CCC: $14.00

is the primary determinant of the oligomeric structure and the common functional features (*16, 17*). While it has been shown that the α-crystallin domains of both HSP 27 and αB-crystallin are able to assemble into large oligomeric aggregates, these separate domains have no chaperone-like activity (*18*). The recent isolation of a monomeric sHSP from *C. elegans* consisting of one domain showing sequence similarity to the α-crystallin domain suggests a critical role for the N-terminal region in the assembly of the oligomeric structure (*19*).

The evaluation of the role of the α-crystallin domain and consequent insight into the molecular mechanisms involved in these diverse functions are hampered by the lack of structural information on HSP 27 and sHSPs in general. The major difficulty relates to the considerable flexibility of their quaternary structure (*20*). This flexibility, believed to be critical for their function, results in conformational heterogeneity that to date has prevented the crystallization of these proteins. Therefore, there is limited information concerning the tertiary structure of the subunits and their arrangement in the oligomer. It has been proposed that mammalian sHSPs have a tertiary structure similar to that proposed for lens α-crystallin subunits (*17*). The model, proposed by Wistow, consists of two domains, each of two structurally similar motifs with a dynamic C-terminal arm (*21*). On the secondary structure level, HSP 27 appears to be composed mainly of β-sheets as revealed by far-UV circular dichroism (CD) (*18*). Electron microscopy studies indicate that mouse HSP 25 forms ring-like particles. Behlke et al. proposed that these particles are composed of 32 monomers in hexagonal packing (*22*).

One approach to studying the oligomeric structure of sHSP is site-directed spin-labeling (SDSL) [for a recent review, see (*23*)]. Unlike diffraction techniques, the application of SDSL does not require a crystalline sample and is not limited by the size or molecular complexity of the protein. In SDSL, structural information is obtained from electron paramagnetic resonance (EPR) analysis of a reporter group, a paramagnetic nitroxide spin-label, site-specifically-introduced into the protein sequence. It has been established that sequence-specific variation in the accessibilities and mobilities of attached spin-labels can be used to map the location of secondary structural elements and their orientation relative to the protein fold (*23, 24*). The relative arrangement of the secondary structural elements and the location of interfaces between protein domains and/or subunits can be deduced from analysis of spin−spin interactions between pairs of nitroxides (*25*−*28*). In previous work, SDSL was employed to determine secondary structure and solvent accessibility along a conserved sequence in αA-crystallin. It was concluded that a β-strand spans the sequence and that equivalent strands from different subunits are in close proximity in the oligomer (*29*).

In this paper, we extend this line of investigation to the equivalent sequence in the α-crystallin domain of HSP 27 between amino acids 133 and 144. This is the first sequence-correlated structural comparison of two sHSPs. The goals of this comparison are to map the location of the putative structural core in sHSP and to understand the extent to which such a core determines the fold of individual subunits and their symmetry in the oligomer. Our data are consistent with a β-strand configuration along the sequence and identify a subunit interface in the α-crystallin domain of HSP 27. These results, in conjunction with the results of Berengian et al. (*29*) on the equivalent sequence in αA-crystallin, indicate that in both proteins the assembly of the oligomeric structure involves a conserved element of symmetry.

EXPERIMENTAL PROCEDURES

Materials. The cDNA of human HSP 27 was obtained from Stressgen. Spin-label I was a generous gift from Professor Kalman Hideg, University of Pécs, Hungary. NiEDDA was kindly provided by Dr. Christian Altenbach, University of California, Los Angeles. Bovine insulin was from Sigma. Source Q media, Superose 6, and HiTrap columns were from Pharmacia Biotech. Tris(2-carboxyethyl)phosphine (TCEP) was obtained from Molecular Probes.

Site-Directed Mutagenesis. The cDNA of HSP 27 was cloned into the *Nde*I and *Xho*I sites of the plasmid pET-20b+. Using DNA sequencing, we verified that the cloned DNA coded for an identical amino acid sequence to those deposited in GenBank under Accession Numbers X54079 and Z23090. To perform site-directed mutagenesis, a new unique *Xma*I site was introduced at position 441 in the nucleotide sequence. Antisense primers containing the desired X→cysteine substitution and overlapping the *Xma*I site were used in conjunction with a sense primer overlapping a unique *Hin*cII site to generate PCR fragments. The fragments were then digested and subcloned. For all mutant constructs, the entire amplified portion of the gene was sequenced to confirm the substitution and the absence of unwanted changes. Single-site mutants are named by specifying the original residue, the number of the residue, and the new residue, in that order. The HSP 27 base mutant containing the C137A substitution is referred to as WT*.

Expression and Purification of HSP 27 Mutants. Mutant plasmids were used to transform competent *E. coli* BL21-(DE3). Cultures, inoculated from overnight seeds, were grown to midlog phase at 37 °C. Then the temperature was lowered to 30 °C, and the expression of HSP 27 was induced by the addition of 0.4 mM IPTG. After 4 h of induction, the cells were harvested by centrifugation and resuspended in a lysis buffer containing 20 mM Tris, 1 mM EDTA, 75 mM NaCl, and 10 mM DTT, pH 8.0. The resuspended cultures were then disrupted by sonication, and the DNA was precipitated by the addition of 0.06% poly(ethylenimine). The lysates were then centrifuged at 15000*g* and loaded on a source Q column. The column was washed with 10 volumes of buffer A containing 50 mM Tris, 1 mM EDTA, and 75 mM NaCl, pH 8.0. Then the fraction containing HSP 27 was eluted with a gradient of 0.1−1 M NaCl in buffer A. The peak containing HSP 27 was further purified by gel filtration on a Superose 6 column. Sample purity was analyzed by SDS−PAGE and found to be better than 90%. Absolute protein concentrations were determined by UV absorption using an extinction coefficient $\epsilon^{280}_{0.1\%} = 1.9$. Relative protein concentrations were verified using the Bradford assay.

Spin-Labeling of HSP 27 Mutants. Typically, HSP 27 mutants were incubated with a 5-fold excess of spin-label I to generate the side-chain R1 as shown in Figure 1 (*30*). The reaction was allowed to proceed at room temperature for 2 h, and then overnight at 4 °C. The samples were desalted to remove unreacted spin-labels using a HiTrap column.

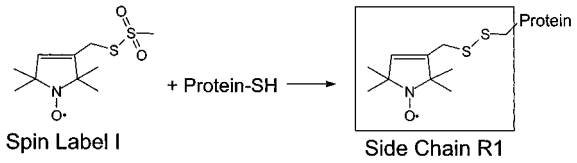

FIGURE 1: Reaction of spin-label I to generate the nitroxide side-chain R1.

The labeling efficiency was determined using an assay suggested by Dr. David Farrens, Oregon Health Sciences University. Conventional methods measure spin concentration using double integration of the spectral line shape and comparison with a standard sample. However, for severely broadened samples where the signal to noise is inherently low, we found relatively significant errors using that method. Therefore, the attached spin-label was released by incubation of a ≈400 μM solution of each spin-labeled mutant with a 1000-fold excess of TCEP (*31*). The amplitude of the central resonance line was measured and the spin concentration obtained from a calibration curve. The calibration curve, relating the amplitude of the central line to spin concentration, was constructed from fresh spin-label solutions prepared in the same buffer in the presence of the same concentration of TCEP. We found that TCEP did not reduce the nitroxide group over a period of 1 h. Using this assay, we verified that all mutants, particularly in the 134−139 stretch, were labeled with at least 90% efficiency.

Circular Dichroism. CD analysis was performed on a Jasco 710 spectropolarimeter. Measurements were taken at room temperature in the range of 190−260 nm. Protein samples were prepared in 20 mM phosphate, pH 7.1, at a concentration of 0.2 mg/mL.

Chaperone Assays. Aggregation of the insulin B chain was monitored by measuring the absorption due to scattering at 360 nm. Insulin, dissolved in 50 mM sodium phosphate, 100 mM NaCl at a concentration of 0.4 mg/mL, was reduced with 20 mM DTT in the presence of variable amounts of WT or mutants HSP 27.

EPR Measurements. Samples for EPR spectroscopy were prepared in 20 mM MOPS, 50 mM NaCl, and 0.1 mM EDTA, pH 7.2. EPR spectroscopy was performed on a Varian E102 spectrometer fitted with a two-loop one-gap resonator (*32*). Samples were loaded in 0.64 mm i.d. gas-permeable-TPX capillaries. The microwave power was 2 mW incident, and the Zeeman modulation amplitude was 2 G. Using a value of 6 for the resonator efficiency parameter Λ reported by Hubbell et al. (*32*), the microwave field at the sample was calculated to be ≈0.25 G.

Power saturation measurements for R1-labeled HSP 27 mutants were carried out under nitrogen and in the presence of 3 mM NiEDDA, and the data were analyzed in terms of the parameter $P_{1/2}$ (*33*). The EPR accessibility parameter, Π, was calculated as previously described except that changes in $\Delta P_{1/2}$ were normalized to a DPPH powder sample (*34*).

RESULTS

Characterization of the Mutants. Eleven consecutive cysteine mutants, spanning the region between Y133 and L144 of the human HSP 27 sequence, were constructed in a cysteine-less "base" mutant. For that purpose, the single native cysteine residue at position 137 was replaced with an alanine. The choice of alanine for substitution was to avoid drastic changes in steric volume, hydrophobicity, and conformational preferences. Although a cysteine residue occurs at position 137 in rat, mouse, and hamster HSP 25/27, this residue is not conserved across the sHSP family. The corresponding residue in the α-crystallins is a glutamate (*2*).

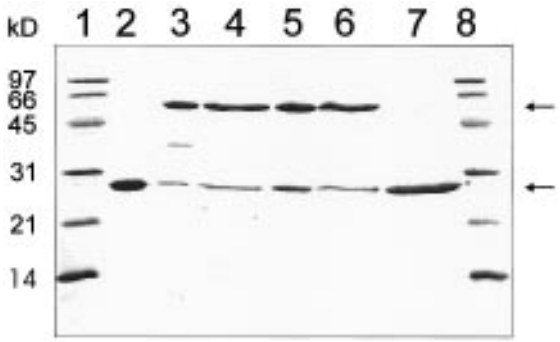

FIGURE 2: SDS−PAGE analysis of oxidized WT HSP 27. Lane 2, HSP 27 in the presence of DTT. Lane 3, HSP 27 incubated at 4 °C overnight. Lanes 4−6, oxidation with Cu-phenanthroline, lane 4 in the presence of 50-fold molar excess for 15 min, lane 5 in the presence of 20-fold molar excess for 15 min, lane 6 in the presence of 50-fold molar excess for 60 min. Lane 7 is the sample in lane 6 in the presence of DTT.

While previous studies employed HSP 25/27 expressed in *E. coli*, there have been no published experimental data on whether the native cysteine is involved in intersubunit disulfide bonds. One of the indications that the native cysteines from different subunits are in close proximity to form such a bond is shown in Figure 2. Purified WT HSP 27 at a nominal oligomer concentration of 1 μM was incubated with a 50-fold molar excess of Cu-phenanthroline (*35*). The reaction was allowed to proceed for 15 min at 4 °C and then stopped by the addition of EDTA. Figure 2 shows that a significant population of dimers forms, indicating that the two cysteines are in relatively close proximity. Cross-linking was also observed, although with slower kinetics, in the presence of a redox buffer consisting of different molar ratios of oxidized to reduced glutathione (not shown). In all cases, reduced glutathione was in excess to prevent the nonspecific formation of interoligomer disulfide bonds. In the absence of DTT and EDTA, incubation of WT HSP 27 overnight at 4 °C resulted in almost complete conversion into the dimeric species (Figure 2, lane 3).

Despite the possibility that the formation of such a disulfide bridge can increase the stability of HSP 27 in vivo, we speculated that it cannot be critical for room temperature structure and chaperone activity for two reasons. First, previous structural and functional studies have used HSP 25/27 expressed in *E. coli*. The highly reducing environment in the cytoplasm usually does not allow the formation of disulfide bonds. Furthermore, most purification protocols and chaperone assays were carried out in the presence of DTT. Second, the cysteine is not conserved across the small heat-shock protein family.

In agreement with the above analysis, the C137A substitution did not result in any significant changes in the ability of HSP 27 to suppress the chemically induced aggregation of the insulin B chain at room temperature. As reported previously, the B chain aggregates following the reduction of the insulin interchain disulfide bonds (*36*). This can be detected by absorption due to light scattering at 360 nm. The

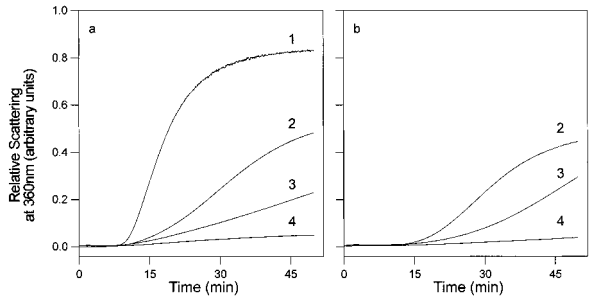

FIGURE 3: Chaperone-like activity of (a) WT and (b) WT*. The insulin to HSP 27 weight ratios are as follows: curve 1, 1:0; curve 2, 1:0.125; curve 3, 1:0.25; curve 4, 1:0.5.

Table 1: Average Molecular Masses of R1-Labeled HSP 27 Mutants

mutant	molecular mass (MDa) ± 0.03	mutant	molecular mass (MDa) ± 0.03
WT	0.57	141	0.64
WT*	0.57	142	0.66
133	0.64	143	0.62
134	0.70	144	0.67
135	0.62	134ex[a]	0.62
136	0.67	135ex[a]	0.60
137	0.56	136ex[a]	0.62
138	0.72	137ex[a]	0.60
139	0.63	138ex[a]	0.57
140	0.70	139ex[a]	0.58

[a] In the presence of a 4-fold molar excess of WT*.

rationale for using the insulin assay is that it is conducted at room temperature where most of the mutants are thermodynamically stable. Figure 3a shows that WT HSP 27 delays the onset of aggregation and reduces its rate. A weight ratio of 1:0.5 is sufficient to suppress the aggregation of the B chain. Figure 3b also shows that the chaperone-like activity of the WT* variant is indistinguishable from the WT. In fact, all cysteine mutants were at least as efficient as the WT with respect to chaperone-like activity.[2] The efficiency of all even mutants was evaluated by comparing the effect of different concentrations on the aggregation of the B chain relative to that of the WT (not shown).

Gel filtration chromatography was used to assess the ability of the spin-labeled mutants to assemble into large molecular mass oligomers. At the concentration and injection volumes reported, all mutants migrated as a predominant single peak on a Superose column, indicating the absence of significant dissociation of the oligomer. The elution volumes were then used to estimate the *apparent* average molecular mass of each oligomer. The data, shown in Table 1, indicate that unlabeled WT HSP 27 migrates as a 570 kDa oligomer. Remarkably, R1-labeled WT as well as the WT* variant have identical apparent molecular mass, within the experimental error, as the unlabeled WT.

However, the apparent molecular mass of R1-labeled mutants shows considerable variability particularly for the even mutants, i.e., 134, 136, ..., 144. Similar changes in the apparent molecular mass were observed upon the R1 substitution of the corresponding residues in αA-crystallin (*29*). The deviations appear to be largest at residues 138 and 140, both of which are highly conserved across the sHSP family. While it is possible that changes in the number of subunits are at the origin of the observed deviations in molecular mass, the more likely interpretation is a change in the hydrodynamic radius of the oligomer due to limited structural rearrangements induced by the mutation at a packing interface. Such an interpretation is consistent with the location of residues 134−139 near a surface of subunit contacts revealed by the EPR analysis below.

The overall structural integrity of each R1-labeled mutant relative to the WT was measured by far-UV circular dichroism. Figure 4a shows that the CD spectrum of the WT* variant is superimposable on that of the WT. The R1-labeled mutants were divided into two classes based on their effects of the global secondary structure. Overall the spectra of the odd mutants, shown in Figure 4b, have the characteristic shape of WT HSP 27 with a minimum at 217 nm, indicating little if any structural perturbation. The spectra of the even mutants, on the other hand, reveal structural destabilizations that appear to be particularly pronounced at residues 138 and 140. The spectra show changes in the 190−200 nm region usually associated with mutations that affect the packing of secondary structural elements (Figure 4c).

Tertiary and Quaternary Interactions along the Sequence. Figure 5 shows the room temperature EPR spectra of the R1-labeled HSP 27 mutants. All spectra were normalized, by double integration, to represent the same number of spins. Therefore, the variation in the spectral intensity reflects changes in mobility and/or spin−spin interactions as R1 is scanned across the sequence. The spectra of R1 at residues 134−139 show clear evidence of spin−spin interactions between labels in close proximity (*26*). The line shapes are characterized by the presence of spectral intensities separated by more than 100 G and by a marked drop in the overall intensity. The spectrum of F138R1 shows distinct splitting that can only arise from highly oriented, interacting spin-labels with no relative motion and little if any static disorder. Since each label is on a different subunit, the spectral broadening indicates that these residues are along or close to an interface between subunits.

That spin−spin interactions result from the assembly of subunits in the quaternary structure was further confirmed by refolding the mutant oligomers in the presence of excess WT*. Figure 6 shows the EPR spectra of R1 in the spin-diluted oligomers. In each case, the spin−spin interaction is largely eliminated as indicated by the increase in the spectral intensity and the decrease of the overall spectral width. For mutants I134R1 and F138R1, it was necessary to add a 6-fold molar excess of WT* compared to 4-fold excess for the rest of the mutants. Despite the added molar excess of WT*, the spectra of I134R1 and F138R1 showed residual spin−spin interaction. We speculate that the destabilization of these mutants, evident in their CD spectra, results in a less favorable interaction with WT* subunits, thus promoting the aggregation of R1-labeled subunits. We were able to completely suppress the spectral features arising from spin−spin interactions by labeling one of every six subunits in the I134R1 oligomer (not shown).

The elimination of the spectral broadening allows the analysis of the mobility of R1 at sequential residues. The mobility of R1, encoded in the spectral line shape, reflects rotational isomerization about the bonds that link the nitroxide to the protein backbone and has contributions from

[2] Under our conditions, the chaperone-like efficiency of WT and HSP 27 mutants varied by as much as 20%. Thus, mutants displaying efficiency within 30% of WT were considered fully active.

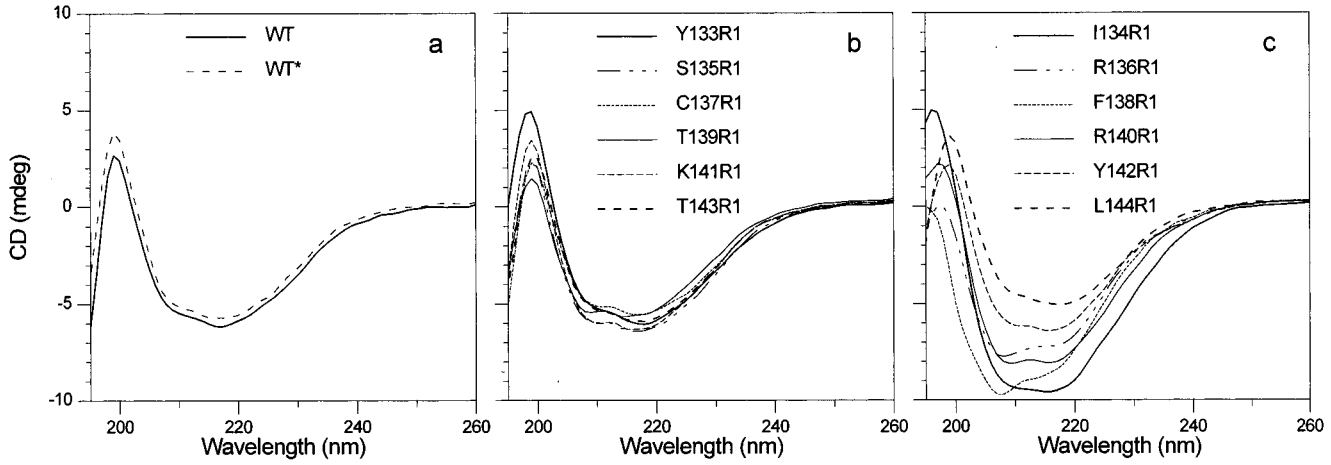

FIGURE 4: Far-UV circular dichroism spectra of HSP 27 and its mutants. Measurements were made at a protein concentration of 0.2 mg/mL in 20 mM sodium phosphate using a 0.1 cm path length cuvette. Spectra were the average of 16 scans.

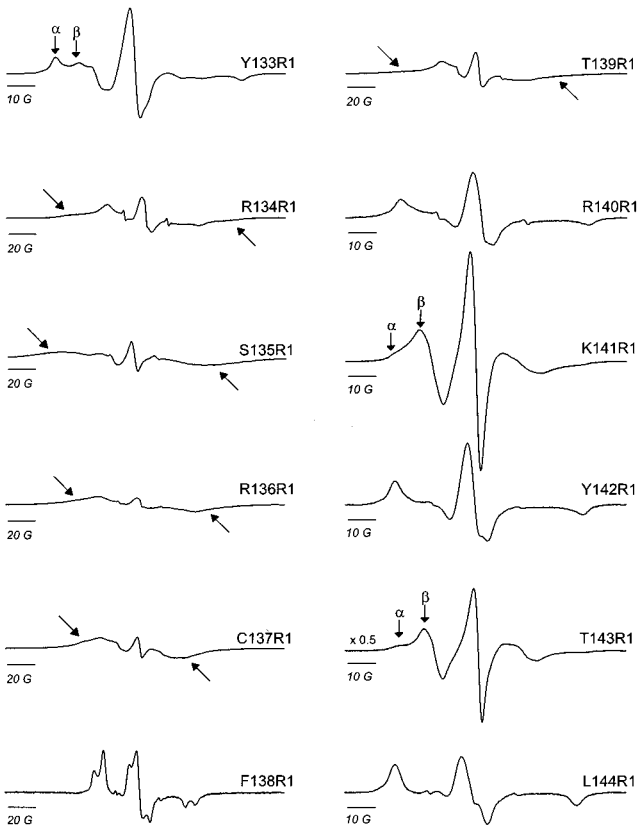

FIGURE 5: Room temperature EPR spectra of R1-labeled HSP 27 mutants. The spectra were normalized to represent the same number of spins. All spectra were recorded with a 100 G scan width except 134−139, which have a scan width of 200 G. The spectrum of T43R1 was scaled by a factor of 0.5 for convenience of representation.

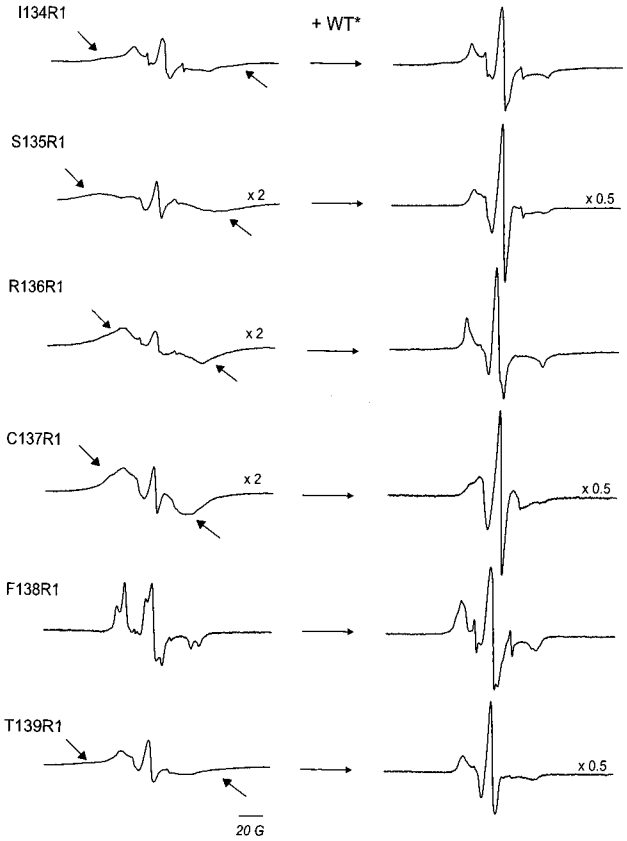

FIGURE 6: Room temperature EPR spectra of R1-labeled HSP 27 mutants in the presence of molar excess WT*. All spectra were recorded with a 200 G scan width. They were normalized by double integration to represent the same number of spins. The broadened spectra were scaled to show the details of the line shape. The scaling factor is shown to the right of each spectrum.

the motion of the backbone relative to the average structure. The effect of the overall oligomer tumbling is negligible on the nanosecond time scale (*37*). Steric interactions of the nitroxide with the protein fold modulate R1 mobility in a manner that reflects primarily tertiary and, for oligomeric proteins, quaternary interactions. Thus, in Figure 5, the periodic change in the spectral line shape observed between residues 140−144 indicates the presence of two distinct sets of structural constraints. The spectra of R1 at 140, 142, and 144 reveal little motion of the nitroxide relative to the protein matrix at these sites and are characteristic of nitroxides in a highly ordered environment. They are exclusively observed at sites buried in the protein's hydrophobic core (*37*). The mobility of R1 at 141 and 143, on the other hand, is significantly less restricted as is apparent from the increase in the spectral amplitude. The line shape indicates the presence of two components with distinct rotational mobility, identified as α and β in Figure 5. Such spectra are normally associated with steric contact sites although they also can be observed at exposed sites (*37*). Measurement of the solvent accessibility of R1 at these sites is necessary to distinguish between these two possibilities.

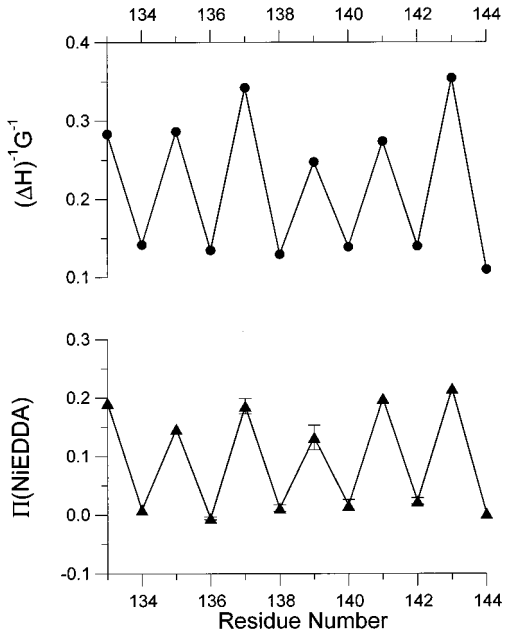

FIGURE 7: Sequence-specific environmental parameters of R1. Reciprocal of the central line width, ΔH^{-1} (●), and Π(NiEDDA) (▲) versus the residue number.

The oscillatory behavior is less obvious in sequence 133−139, although it can be inferred from a careful comparison with reference spectra in T4L (*37*). R1 at even sites in this stretch has a near rigid limit line shape consistent with a buried location. The spectra of 133, 135, and 139, on the other hand, have distinct line shapes from those of R1 at the even mutants despite the presence of outer splittings. The increased mobility of R1 at these residues is reflected in the mobile component, the β component in the spectrum of Y133R1, that is not usually observed at sites buried in protein hydrophobic cores (*37*). Thus, the spectra of 133R1, 135R1, and 139R1 indicate steric contacts arising either from tertiary interactions within the fold of a subunit or from quaternary interactions with a neighboring subunit.

The periodic change in the mobility of R1 across the sequence can be graphically summarized by plotting the value of the inverse central line width, ΔH_0^{-1}, as a function of residue number. This parameter is an estimator of the rate and amplitude of the nitroxide motion (*37*). While the values of ΔH_0^{-1} at even residues are indicative of their highly ordered environment, the values at odd residues, particularly in the 133−139 stretch, overestimate the mobility and mask important features of the line shape, i.e., the two-state composite spectrum (*37*). Nevertheless, as R1 is scanned along the sequence, Figure 7 shows a striking oscillatory behavior with a period of 2, indicative of a β-strand.

Solvent Accessibility along the Sequence. Solvent accessibility is deduced from measurement of the collision frequency between R1 and a paramagnetic reagent exclusively present in the aqueous phase. For water-soluble proteins, NiEDDA is used. Because of its polarity and size, this reagent has hardly any solubility in the protein hydrophobic core (*23*). Collision frequencies between the attached nitroxides and NiEDDA are determined from changes in the nitroxide saturation parameters and are expressed by the EPR accessibility parameter, Π (*34*). For the same paramagnetic reagent, Π is inversely related to the local atomic density. Therefore, R1 at buried residues is expected to have small values of Π. Similarly, R1 at sites in steric contacts is expected to have lower Π values than R1 at sites exposed on the surface of the oligomer. R1 scanning through a regular secondary structure, sampling two or more of these environments, results in a periodic pattern in the accessibility profile that identifies the type of the secondary structural element and its orientation (*23*).

Such a periodic pattern is clearly observed in Figure 7. In agreement with mobility data, the plot of Π versus sequence number reveals two distinct structural environments consistent with a β-strand. The oscillation in the mobility and accessibility are in phase, as expected for a regular secondary structural element in a water-soluble protein (*23*). The orientation of the β-strand with respect to the fold can be determined from the phase of the pattern. R1 at even sites across the sequence has small values of Π similar to those observed at sites buried in the hydrophobic core of T4L, indicating that the even residues form the more buried face of the strand. The other face of the strand, consisting of the odd residues, has relatively higher Π values, indicating partial solvent accessibility. Furthermore, the absolute values of Π do not suggest that the odd residues are exposed on the surface of the oligomer. This is consistent with the lineshape analysis assigning residues 133, 135, and 139 as steric contact sites. Only small differences in Π values between residues 141 and 143 and the rest of the odd residues were detected despite the somewhat different line shape. The possible origin of this difference is addressed under Discussion.

DISCUSSION

A nitroxide scan was performed along a highly conserved sequence in the α-crystallin domain of HSP 27 between residues 133 and 144. The sequence was selected based on the multiple sequence alignment of de Jong and co-workers showing that residues 138, 140, and 144 are conserved across the sHSP family (*17*) and the results of Berengian et al. (*29*) demonstrating that the equivalent sequence in αA-crystallin is located near a subunit interface. The objectives of the reported study were: (1) to evaluate the role of the residues in the chaperone-like function of HSP 27, (2) to determine the secondary structure and solvent accessibility along the sequence, and (3) to examine whether these residues are involved in intersubunit contacts.

Structural and Functional Consequences of the Mutations. The pattern of perturbation due to residue substitution along the sequence has a biphasic periodicity as a function of the sequence position. The effect of the substitution on the apparent average molecular mass (Table 1) and the global secondary structure (Figure 4) is particularly pronounced at the even residues, consistent with the buried location of these residues as revealed by EPR analysis (*38*). It is also consistent with the stringent conservation of residues F138 and R140 in distant members of the sHSP family (*2*). At these residues, R1 substitutions are expected to result in local repacking to accommodate the increased volume of R1 (*39*). Thus, the changes in the elution volumes are probably due to alterations in the hydrodynamic radius induced by the substitution of these residues. In this context, the structural perturbation observed due to the substitution of the two charged residues 136 and 140 suggests that buried salt bridges are involved in the assembly of the HSP 27 structure.

Charged residues, particularly arginines, are frequently observed near subunit interfaces and are involved in salt bridges and hydrogen bonds (*40*).

Remarkably, all mutants were as efficient as the WT in suppressing the aggregation of the insulin B chain at room temperature. This result is similar to that obtained for the corresponding mutants in αA-crystallin (*29*). Even mutants with altered far-UV CD spectra have chaperone-like activity similar to that of the WT, at room temperature. This is consistent with a mechanism of chaperone-like function where substrate binding occurs at exposed hydrophobic residues rather than in buried regions of the oligomer (*41*).

The chaperone-like efficiency of HSP 27 appears to be 1 order of magnitude higher than that of αA-crystallin *at room temperature*. On a monomer to monomer basis, HSP 27 binds around five insulin molecules more than αA-crystallin. Such a difference in chaperoning efficiency was already noted between αA- and αB-crystallins [J. Horwitz, personal communication, (*42*)].

Structure along the 134−*144 Sequence*. Analysis of mobility and solvent accessibility along the sequence reveals the presence of two distinct structural environments. The even residues are all in a buried environment with a structural order similar to that observed for residues located in the interior of proteins. At these sites, there is little or no motion of R1 relative to the oligomer, and there is virtually no accessibility to the polar reagent NiEDDA, exclusively present in the aqueous phase. The odd residues, on the other hand, are partially accessible to NiEDDA. The spectral line shapes of R1 at these residues show a range of mobilities that nonetheless indicate a distinct structural environment from that of the even residues. Thus, as R1 is advanced along the sequence, it alternates between the two environments with a period of 2. That this periodicity is characteristic of a β-strand has been established in cellular retinol binding protein (*23*). Therefore, we deduce that the backbone conformation along the sequence is consistent with that of a β-strand. The strand is flanked on one side by a glycine (G132) and on the other side by multiple prolines (P145 and P146).

The Π values of R1 at odd residues fall within a narrow range that is similar to that observed at steric contact sites in the monomeric protein T4 lysozyme. Given that residues 134−139 appear to be near a subunit interface (see below), it is likely that the motional restriction of the nitroxide is due to steric contacts of R1 with the fold of a neighboring subunit. The structural assignment of residues K141 and T143 is less clear. As mentioned under Results, there is a notable change in the spectral line shape of R1 at these residues compared to 133, 135, and 139. In general, the structural determinants of the R1 line shape in a β-strand have not been examined in detail. A preliminary report indicates that the mobility of R1 on the more exposed surface is dependent on the right-handed twist characteristic of β-strands in proteins (*43*). By progressively curving the side chain along the strand, the twisting can result in a change in the steric constraints sensed by the R1 side chain. Thus, a possible structural origin of the less restricted motion observed at K141R1 and T143R1 is a twist along the strand.

Interaction between the Strands in the Oligomer. Spin−spin interactions between R1 side chains at identical residues in the 134−139 stretch indicate that equivalent strands from different subunits are in close spatial proximity. For residues

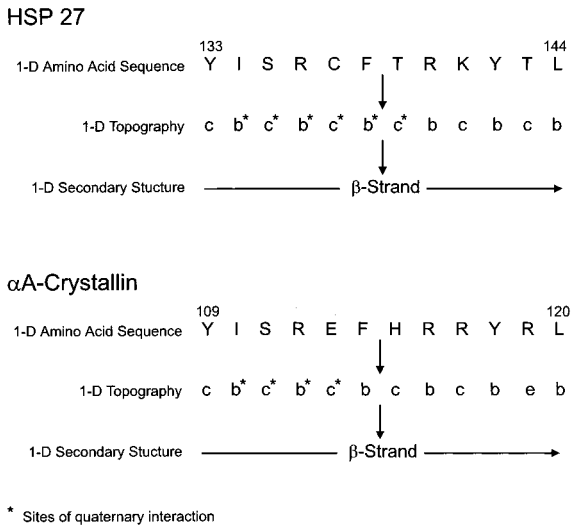

FIGURE 8: Structure along the studied sequence in (a) HSP 27 and (b) αA-crystallin. The letters e, c, and b refer to the exposed, steric contact, and buried structural classes, respectively.

135−137, the interaction results in distinct spectral features such as the appearance of intensities separated by more than 100 G. Generally, such features are only observed when the nitroxides are separated by less than 12 Å. The primary mechanisms of interactions are static dipolar coupling and through space spin-exchange. Preliminary spectral simulation using a convolution method (*25*) and full Hamiltonian analysis (*28*) indicates that the separation between R136R1 from different subunits is ≈10 Å (Hustedt and Mchaourab, unpublished results). However, the analysis assumed two interacting spins, i.e., a dimer interface, and that the nitroxide at 136 is rotationally immobile. The problem is further complicated by the possibility of distance modulation by the internal dynamics of the oligomer and the possibility of a distribution of distances and orientations between the nitroxides. In order to carry out complete spectral simulations, further experiments are needed to determine the number of interacting spins and their symmetry. However, for the purpose of identification of spatial proximity, the analysis presented in Figure 6 is adequate.

Our results showing subunit contacts in the C-terminal domain are in agreement with the results of Merck et al. (*18*), where the recombinant C-terminal domain was found to assemble into large molecular weight aggregates, and the model proposed by Wistow (*16*) suggesting intersubunit contacts in the α-crystallin domain. Furthermore, the observation that equivalent strands from different subunits are in close proximity implies subunit interactions possessing specific elements of symmetry. The simplest symmetry is a 2-fold rotation that results in the hydrogen bonding of the two strands in an antiparallel fashion or their interaction at right angles similar to that seen in prealbumin (*44*). Heterologous association between four monomers to form a closed tetrameric structure can also result in the interaction between identical surfaces. Experiments are currently underway to distinguish between these two possibilities.

Conclusion: Sequence-Correlated Structural Comparison of HSP 27 and αA-Crystallin. Figure 8 summarizes the results of this study in the form of one-dimensional strings of structural parameters where e, c, and b refer to the exposed, steric contact, and buried structural classes, respectively. Also shown in Figure 8 are the results from the study

on the equivalent sequence in αA-crystallin (*29*). In both proteins, the variations in the sequence-specific accessibility and mobility are consistent with a β-strand configuration along the sequence. One face of the strand, including two conserved arginine residues, is buried with almost no solvent accessibility. Furthermore, the patterns of spin−spin interaction suggest that the strands are at a subunit interface. There are two significant aspects to this structural similarity. First, the conservation of the β-strand is consistent with the hypothesis of a common fold in the α-crystallin domain. Second, because symmetry results from interactions along the sequence, at least one such interaction is present in both oligomers. Thus, our results support the conclusion of Merck et al. (*18*) that the formation of a mixed aggregate between αA-crystallin and HSP 27 implies similar quaternary structures.

Given that the sequence appears to be conserved among mammalian sHSPs and lens α-crystallins, it is likely that the subunit interactions resulting in the formation of this subunit interface are critical for the assembly of the native oligomer or a more basic multimeric unit. The extent to which this interface is invariant in more distant sHSPs, i.e., with less extensive sequence similarity, can be examined using the sequence-correlated approach to structural comparison presented in this paper.

ACKNOWLEDGMENT

We thank Prof. Joseph Horwitz for helpful discussions and encouragement, Michael Bova for help with the insulin assay, Dr. David Farrens for suggestion of the labeling-efficiency assay, and Prof. James Hyde for critical reading of the manuscript.

REFERENCES

1. Parsell, D. A., and Lindquist, S. (1993) *Annu. Rev. Genet. 27*, 437−496.
2. Caspers, G., Leunissen, J. A. M., and de Jong, W. W. (1995) *J. Mol. Evol. 40*, 238−248.
3. Arrigo, A. P., and Landry, J. (1994) *The biology of heat-shock proteins* and molecular chaperones (Morimoto, R., Tissieres, A., and Georgopoulos, C., Eds.) pp 335−373, Cold Spring Harbor Laboratory Press, Cold Spring Harbor, NY.
4. Horwitz, J. (1992) *Proc. Natl. Acad. Sci. U.S.A. 89*, 10449−10453.
5. Jakob, U., Gaestel, M., Engel, K., and Buchner, J. (1993) *J. Biol. Chem. 268*, 1517−1520.
6. Bendorf, R., Ryazantsev, S., Wieske, M., Behlke, J., and Lussch, G. (1994) *J. Biol. Chem. 269*, 20780−20784.
7. Lee, G. J., Pokala, N., and Vierling, E. (1995) *J. Biol. Chem. 270*, 10432−10438.
8. Ehrnsperger, M., Gräber, S., Gaestel, M., and Buchner, J. (1997) *EMBO J. 16*, 221−229.
9. Lee, G. J., Roseman, A. M., Saibil, H. R., and Vierling E. (1997) *EMBO J. 16*, 659−671.
10. Klemenz, R., Fröhli, E., Steiger, R. H., Schäfer, R., and Aoyama, A. (1991) *Proc. Natl. Acad. Sci. U.S.A. 88*, 3652−3656.
11. Aoyama, A., Fröhli, E., Schäfer, R., and Klemenz, R. (1993) *Mol. Cell. Biol. 13*, 1824−1835.
12. Mehlen, P., Preville, X., Chareyron, P., Briolay, J., Klemenz, R., and Arrigo, A.-P. (1995) *J. Immunol. 154*, 363−374.
13. Mehlen, P., Schulze-Osthoff, K., and Arrigo, A.-P. (1996) *J. Biol. Chem. 271*, 16510−16514.
14. Mehlen, P., Mehlen, A., Guillet, D., Preville, X., and Arrigo, A.-P. (1995) *J. Cell. Biochem. 58*, 248−259.
15. Chothia, C., and Lesk, A. M. (1986) *EMBO J. 5*, 823−826.
16. Wistow, G. (1993) *Exp. Eye Res. 56*, 729−732.
17. de Jong, W. W., Leunissen, J. A. M., and Voorter, C. E. M. (1993) *Mol. Biol. Evol. 10*, 103−126.
18. Merck, K. B., Groenen, P. J. T. A., Voorter, C. E. M., de Haard-Hoekman, W. A., Horwitz, J., Bloemendal, H., and de Jong, W. W. (1993) *J. Biol. Chem. 268*, 1046−1052.
19. Leroux, M. R., Ma, J. B., Bateleir, G., Melki, R., and Candido, P. M. (1997) *J. Mol. Biol. 272*, 12847−12853.
20. Groenen, P. J. A., Merck, K., de Jong, W. W., and Bloemendal, H. (1994) *Eur. J. Biochem. 225*, 1−19.
21. Wistow, G. (1985) *FEBS Lett. 181*, 1−6.
22. Behlke, J., Lutsch, G., Gaestel, M., and Bielka., H. (1991) *FEBS Lett. 288*, 119−122.
23. Hubbell, W. L., Mchaourab, H. S., Altenbach, C., and Lietzow, M. A. (1996) *Structure 4*, 779−783.
24. Hubbell, W. L., and Altenbach, C. (1994) *Curr. Opin. Struct. Biol. 4*, 566−573.
25. Rabenstein, M. D., and Shin, Y. K. (1995) *Proc. Natl. Acad. Sci. U.S.A. 92*, 8239−8243.
26. Mchaourab, H. S., Oh, K. J., Fang, C. J., and Hubbell, W. L. (1997) *Biochemistry 36*, 307−316.
27. Farrens, D. L., Altenbach, C., Hubbell, W. L., and Khorana, H. G. (1996) *Science 274*, 768−770.
28. Hustedt, E. J., Smirnov, A. I., Laub, C., Cobb, C. E., and Beth, A. H. (1997) *Biophys. J. 72*, 1861−1877.
29. Berengian, A. R., Bova, M. P., and Mchaourab, H. S. (1997) *Biochemistry 36*, 9951−9957.
30. Berliner, L. J., Hankovsky, H. O., and Hideg, K. (1982) *Anal. Biochem. 119*, 450−453.
31. Burns, J. A., Butler, J. C., Moran, J., and Whitesides, G. M. (1991) *J. Org. Chem. 56*, 2648−2650.
32. Hubbell, W. L., Froncisz, W., and Hyde, J. S. (1987) *Rev. Sci. Instrum. 58*, 1879−1886.
33. Altenbach, C., Flitsch, S., Khorana, H. G., and Hubbell, W. L. (1989) *Biochemistry 28*, 7806−7812.
34. Farahbakhsh, Z. T., Altenbach, C., and Hubbell, W. L. (1992) *Photochem. Photobiol. 56*, 1019−1033.
35. Kobashi, K. (1968) *Biochim. Biophys. Acta 158*, 239−245.
36. Farahbakhsh, Z. T., Huang, Q., Ding, L., Altenbach, C., Steinhoff, H., Horwitz, J., and Hubbell, W. L. (1995) *Biochemistry 34*, 509−516.
37. Mchaourab, H. S., Lietzow, M. A., Hideg, K., and Hubbell, W. L. (1996) *Biochemistry 35*, 7692−7704.
38. Matthews, B. W. (1995) *Adv. Protein Chem. 46*, 249−278.
39. Lim, W. A., Farrugio, D. C., and Sauer, R. T. (1992) *Biochemistry 31*, 4324−4333.
40. Janin, J., Miller, S., and Chothia, C. (1988) *J. Mol. Biol. 204*, 155−164.
41. Smulders, R. H. P. H., Merck, K. B., Aendekerk, J., Horwitz, J., Takemoto, L., Slingsby, C., Bloemendal, H., and de Jong, W. W. (1995) *Eur. J. Biochem. 232*, 834−838.
42. Sun, T. X., Das, B. K., and Liang, J. N. (1997) *J. Biol. Chem. 272*, 6220−6225.
43. Lietzow, M. A., and Hubbell, W. L. (1997) *Protein Sci. 6*, 112.
44. Blake, C. C. F., Geisow, M. J., Swan, I. D. A., Rerat, C., and Rerat, B. (1974) *J. Mol. Biol. 88*, 1−12.

BI971700S